

# Temporal analysis of laser-induced plasma properties as related to laser-induced breakdown spectroscopy

V. Hohreiter, J.E. Carranza<sup>1</sup>, D.W. Hahn\*

*Department of Mechanical and Aerospace Engineering, University of Florida, Box 116300, Gainesville, FL 32611-6300, USA*

Received 10 October 2003; accepted 23 December 2003

## Abstract

The evolution of a laser-induced plasma is characterized in terms of its temporally resolved spectral absorptivity, spectral emissivity, and free electron density via Stark broadening during the first few hundreds of nanoseconds. Transmission measurements using 532 and 1064 nm probe laser beams reveal near opacity of the laser-induced plasma at times corresponding with the tail end of the plasma creating laser pulse. This temporal region is coincident with the maximum free electron density greater than  $10^{18} \text{ cm}^{-3}$ . At times approaching 500 ns following plasma initiation, the plasma absorptivity diminishes markedly, rendering the plasma essentially transparent to incident radiation. The fundamental change from an absorbing (i.e. optically thick) plasma to a non-absorbing plasma during this period is important with respect to the radiative transfer within and from the plasma. Overall, these phenomena play important roles in the evolution of the laser-induced plasma and the technique of laser-induced breakdown spectroscopy.

© 2004 Elsevier B.V. All rights reserved.

*Keywords:* Laser-induced; Plasma; Spectroscopy

## 1. Introduction

The analysis of aerosol particles has been addressed recently using the technique of laser-induced breakdown spectroscopy (LIBS) [1,2]. It is widely known that the LIBS technique uses a highly energetic micro-plasma to vaporize and dissociate matter within the laser-induced plasma, including engulfed particles. However, less is known, both theoretically and experimentally, with regard to the interactions between the laser-induced plasma and particles. In a recent study, research efforts were focused to quantify these plasma–particle interactions pursuant to quantitative LIBS-based analysis [3]. It was found that individual silica particles up to 2  $\mu\text{m}$  in diameter were completely vaporized in the laser-induced plasma and yielded a linear response, while larger particles revealed a less than linear response with

respect to analyte atomic emission presumably due to incomplete vaporization. While the plasma–particle interaction is not well understood, it appears that the transient nature of the plasma in the early stage of plasma evolution plays an important role in the vaporization process [3]. Hence, rate limitations may be more important than simple plasma and particle heat capacities. Accordingly, as a first step toward understanding the plasma–particle processes, it is important to characterize laser-induced plasmas in the early stages of evolution. To further advance this understanding, this paper studies the plasma evolution via time-resolved measurements of electron number density, plasma absorptivity, and plasma continuum emission.

Laser-induced plasmas have been studied using parameters such as electron temperature, electron density, emission intensity, etc. Parigger et al. [4] studied the decay of plasmas produced in hydrogen by a Nd:YAG laser (1064 nm) using the hydrogen Balmer series emission lines. They found that in the first hundreds of nanoseconds following laser breakdown, the free electron density was approximately  $10^{18} \text{ cm}^{-3}$ , and the plasma temperature was approximately 80 000 K (cal-

\*Corresponding author. Tel.: +1-3523920807; fax: +1-3523921071.

E-mail address: [dwhahn@ufl.edu](mailto:dwhahn@ufl.edu) (D.W. Hahn).

<sup>1</sup> Current address: Polytechnic University of Puerto Rico, San Juan, Puerto Rico.

culated using Boltzmann plots), while at times comparable with the plasma-initiating laser pulse electron densities were on the order of  $10^{19} \text{ cm}^{-3}$ . In a more recent study, Parigger et al. [5] further explored Stark-broadened emission profiles in gaseous hydrogen plasmas, comparing both  $H_{\alpha}$  and  $H_{\beta}$  measurements in the context of recent treatments of ion dynamics as reported by Oks [6]. For electron densities in excess of  $10^{17} \text{ cm}^{-3}$ , corresponding to delay times less than 500 ns, agreement between inferred electron density values from  $H_{\alpha}$  and  $H_{\beta}$  profiles was very good. However, at longer delay times some discrepancies were noted when using the standard theoretical treatment per Griem [7,8], while good agreement between the  $H_{\alpha}$  and  $H_{\beta}$  results was achieved with the updated treatment of Stark broadening for electron densities approaching  $10^{16} \text{ cm}^{-3}$ . Borghese et al. [9] measured a plasma kernel of approximately  $0.02 \text{ mm}^3$  as produced by a fundamental Nd:YAG laser in air during the stage of maximum emission (approx. 20 ns following plasma initiation). They calculated a corresponding plasma temperature of approximately 35 000 K at this time using an experimental Planck function, but also calculated higher plasma temperature at earlier times (e.g.  $10^5 \text{ K}$  at approx. 10 ns). Using techniques such as shadowgraphy and interferometry, Villagran-Muniz et al. [10] found that the plasma electron density was approximately  $10^{18} \text{ cm}^{-3}$  for a pulse energy of 300 mJ, and additionally calculated temperatures behind the shock wave (due to the optical breakdown) of approximately  $10^5 \text{ K}$  during the first tens of nanoseconds, when the shock wave is not detached from the plasma. Work by Yalcin et al. investigated plasma temperature and free electron density, including spatially resolved measurements using Abel-inversion, for delay times as early as 350 ns following plasma initiation [11]. Using  $H_{\alpha}$  line widths, they reported peak electron densities of  $1.2 \times 10^{18} \text{ cm}^{-3}$ , and reported little variation (approx. 10%) in this value across the plasma using spatially resolved measurements.

All the available research shows that the plasma in its early stage is a highly energetic system that is characterized by rapid changes, and is not necessarily in thermodynamic equilibrium. For LIBS-based aerosol analysis, these changes need to be assessed in order to identify parameters that could play important roles in the interactions between the plasma and concomitant particles, including free electron densities and plasma absorptivity. In the following sections, the evolution of the laser-induced plasma is assessed based on temporally resolved spectral absorptivity and emissivity measurements, along with evaluation of the free electron density via Stark broadening.

## 2. Experimental methods

A 1064-nm Q-switched Nd:YAG laser operating with 275-mJ pulse energy, 10-ns pulse width, and 5-Hz pulse

repetition rate was used as the plasma source for all experiments. The expanded laser beam (12-mm in diameter) was focused using a 75-mm focal length UV grade plano-convex lens to create an approximately 20- $\mu\text{m}$  diameter focal spot for plasma formation. The plasma emission was collected along the incident beam in a backward direction and separated using a 50-mm diameter elliptical pierced mirror. The collected light was launched into an optical fiber bundle coupled to a spectrometer (2400-groove/mm grating, 0.12-nm optical resolution), and recorded with an intensified charge-coupled device array.

The plasma was formed in an atmospheric pressure gas cell as described previously [12]. A gaseous stream of 42 lpm of purified (HEPA filtered), dry air was passed through the sample cell. For the electron density measurements, an additional flow rate of high purity methane was added to the airflow to enhance the hydrogen emission line signal. The overall methane/air flow rate was maintained at 3% methane, below the lower flammability limit (5%) of methane in air, to prevent ignition by the laser-induced plasma. For the transmission measurements described below, the gas cell windows orthogonal to the plasma-forming laser beam were removed, hence the plasma was formed in the laboratory air. For electron density measurements, Stark broadening of the  $H_{\alpha}$  line was measured. For these measurements, a calibrated blackbody source was used to convert the recorded plasma emission to a relative spectral irradiance scale across the measured spectral bandwidth.

Plasma continuum emission measurements and electron density measurements were based on the spectral analysis of an ensemble average of 100 spectra. For the plasma absorptivity measurements, a probe Nd:YAG laser beam was synchronized to the plasma-creating laser by externally triggering both the flashlamp and Q-switch. The temporal jitter between the plasma-initiating laser pulse and the probe laser pulse was approximately 1 ns. The probe laser was operated using either the frequency-doubled 532-nm line (approx. 6 ns fwhm pulse width), or the fundamental 1064-nm line. The pulse energy of the probe laser was maintained at 15 mJ for both the 532 and 1064-nm probe beams. However, the flashlamp pump energy was significantly reduced for the 1064-nm probe beam, which resulted in a broader temporal pulsewidth, namely  $\sim 30 \text{ ns}$  fwhm.

The probe laser beam was directed orthogonal to the plasma-creating laser beam, and focused at the center of the resulting plasma using a 250-mm focal length lens. The probe laser beam alone had insufficient energy (15 mJ) to create a plasma, which was verified by the absence of breakdown with the probe laser alone, as well as the absence of breakdown at long delay times following the 1064-nm laser initiated plasma. The probe laser was translated both horizontally and vertically until

the minimum transmission was recorded at a delay time of 20 ns with respect to the plasma-initiating 1064-nm laser pulse. The spatial positioning ensured that the probe laser beam was passed through the most optically dense region of the plasma. It is noted that in a previous study using a similar probe beam arrangement, the plasma was found to expand to its characteristic volume of 1.4 mm<sup>3</sup> by 20 ns following plasma initiation [13]. The transmitted probe laser pulse energy was recorded with a volume-integrating calorimeter (25-mm detector area), using a 1-min average at a 5-Hz repetition rate. The detector was placed approximately 0.5 m from the plasma to eliminate any detection of direct plasma emission, which was verified by the lack of signal in the absence of the probe laser. The large detector area functioned to mitigate any effects of beam steering on the recorded transmission, although no probe beam displacement was observed during the experiments.

The probe laser beam transmission was determined as the ratio of the average laser pulse energy transmitted through the plasma divided by the average laser pulse energy recorded in the absence of the laser-induced plasma (i.e. probe laser only). The latter value functioned as the reference pulse energy, and was taken as the average of the values recorded before and after each plasma measurement. The average relative standard deviation of the reference pulse energy was 1.6% for all experiments; hence probe laser energy drift was not significant. All transmission measurements were recorded a minimum of four times for each reported delay time.

### 3. Results and discussion

The time-resolved plasma transmission measurements are presented in Fig. 1 as a function of delay time between the plasma initiating laser and the probe laser. Data are presented for the 532 and 1064-nm probe beams, along with the temporal profile of the plasma-initiating laser pulse as a reference. Zero delay time corresponds to the peak-to-peak temporal alignment of the two lasers. The transmission profiles reveal the rapid increase in plasma opacity, with the minimum transmission values of 9 and 16% recorded 30 and 40 ns following the plasma initiating pulse for the 532-nm and 1064-nm probe beams, respectively. It is noted that the 1064-nm probe laser had a considerably wider pulse width, as discussed above; hence the temporal resolution of the 1064-nm data is less than the 532-nm data. These observed time scales for the rapid increase in plasma absorptivity correspond well with the full-width of the plasma initiating laser pulse, which decays by 99% of its maximum value in 30 ns from the peak intensity. The Fig. 1 data are further analyzed below in the context of electron number density; however, the transmission data alone are evidence that initial plasma processes are

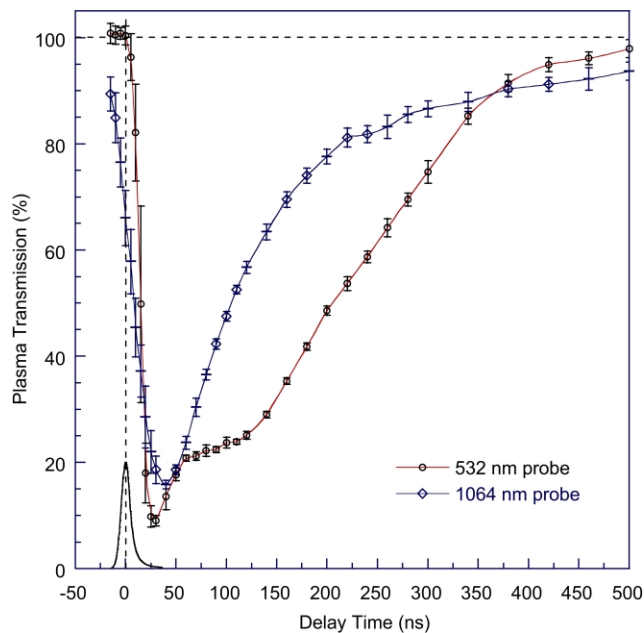


Fig. 1. Plasma transmission as a function of time following plasma initiation using 532 and 1064 nm probe laser beams. The inset laser pulse profile corresponds to the plasma initiating laser pulse at zero delay time.

closely coupled temporally to the plasma initiating laser pulse. The abrupt change in slope of the plasma transmission profile at the tail end of the initiating laser pulse may be interpreted as denoting the change from net plasma energy input to net energy dissipation, the latter for example via radiative transfer and electron recombination (free-bound).

An additional interesting feature of the Fig. 1 data is the return of the plasma transmission to nearly 100% (e.g. 98% and 94% at 532 nm and 1064 nm, respectively) by 500 ns following plasma initiation. This relatively rapid return to an essentially transparent plasma is significant in the context of radiative transfer and in consideration of new LIBS configurations such as dual pulse LIBS. If a second laser beam is to be coupled to an existing laser-induced plasma, temporal delays beyond the first 0.5  $\mu$ s will most likely result in significantly different laser-plasma interactions than those following the first laser pulse within a few hundreds of nanoseconds. The transmission measurements may also be considered in terms of the plasma expansion. As reported in an earlier paper [13], the plasma expands to its characteristic volume of  $\sim 1$  mm<sup>3</sup> within approximately 20 ns, corresponding to an initial plasma propagation velocity on the order of 10 km/s.

Further insight into the plasma processes are revealed by the time-resolved continuum emission measurements presented in Fig. 2. The continuum emission data correspond to the integrated sum of approximately 20 nm bandwidths centered at either 270, 400 or 530 nm. The

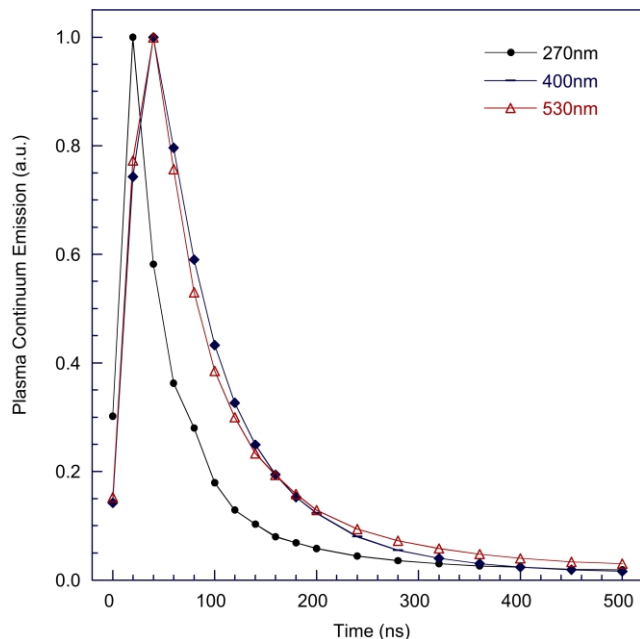


Fig. 2. Plasma continuum emission (20 nm bandwidth) for three spectral regions centered at 270, 400 and 530 nm. All data have been normalized to maximum emission intensity for each respective spectral region.

data are all normalized to their respective maximum temporal emission value. The continuum emission data represent radiative transfer from the plasma, primarily by recombination radiation (free-bound) and Bremsstrahlung emission (free-free). The temporal scale of the continuum emission corresponds markedly with the transmission data discussed above. The continuum emission of all three bands peak between 20 and 40 ns following the peak of the plasma initiating laser pulse, with the 270 nm continuum band peaking  $\sim 10$  ns before the peak of the 400 and 530 nm bands. A fixed detector gate of 20 ns was used for all measurements; hence temporal resolution is limited to such a value. For all three spectral bands, the continuum emission was observed to decay by one order of magnitude during the first 200 ns, which represents a decrease in effective blackbody temperature of approximately 70% based on emissive power per the Planck distribution. Although thermodynamic equilibrium is necessary for the plasma radiative transfer to approach the blackbody function, such a 70% decrease in temperature is quite consistent with reported temperature measurements (see above references) over similar time scales.

To better characterize the laser-induced plasma over the time scales discussed above, electron number density measurements were also performed. Electron densities were calculated based on the Stark broadening of the  $H_{\alpha}$  line (656.3 nm), which is well suited to electron density measurements between  $10^{17}$  and  $10^{19}$   $\text{cm}^{-3}$  [7].

Following the work of Griem, the Stark line intensities at full-width half-maximum (fwhm) are related to the electron density through [8]

$$\Delta\lambda_{\text{fwhm}} = 2\alpha_{1/2}(2\pi)(4/15)^{2/3}e(n_e)^{2/3}, \quad (1)$$

where  $\alpha_{1/2}$  is the fractional half-width of the reduced Stark profile,  $e$  is the electron charge ( $4.8032 \times 10^{-10}$  esu), and  $n_e$  is the free electron number density. The present data were reduced using the values of  $\alpha_{1/2}$  as reported by Griem [8], assuming a plasma temperature of 30 000 K. The inversion of electron densities from Stark widths is rather insensitive to temperature, as related to the corresponding reduced line widths. To assess sources of error due to temperature uncertainty in the present data, the measured Stark line widths were also inverted using temperatures of 20 000 and 40 000 K and the corresponding fractional half-widths. Accordingly, the error bars reported with the measured free electron densities represent the maximum error associated with the uncertainty of  $\pm 10$  000 K. The data were also analyzed using the more recent Stark broadening constants reported by Gigoso and Cardenoso [14]. Using the same temperature of 30 000 K, the calculated electron densities were increased by 27% at the maximum value ( $2.6 \times 10^{18}$   $\text{cm}^{-3}$ ) and by 12% at the minimum value ( $8.9 \times 10^{17}$   $\text{cm}^{-3}$ ), with an average increase of 20% over all measurements. Such differences are assumed within the expected absolute accuracy of the reported electron density measurements based on the data analysis as performed in the current study. Finally, as noted above, recent theories have addressed the indirect and direct coupling between electron and ion broadenings and the impact on Stark broadening [6]. Over the range of the current Stark line widths, application of this more generalized theory is expected to change the electron densities by 10–20% based on recent published comparisons [5].

The measured free electron number densities are presented in Fig. 3 as a function of time following the plasma initiating laser pulse. The hydrogen line widths were not sufficiently resolved from the significant continuum emission for times  $< 100$  ns. From 100 to 500 ns following plasma initiation, the free electron number density decreases from  $2.6 \times 10^{18}$   $\text{cm}^{-3}$  to  $< 10^{18}$   $\text{cm}^{-3}$ . As observed by the error bars in Fig. 3, the uncertainty associated with the assumed plasma temperature is greater in the region of more significant Stark broadening, however, even at the greatest electron number density measured the corresponding relative error is approximately 5%. The measured electron density of  $1.2 \times 10^{18}$   $\text{cm}^{-3}$  at a delay of 350 ns is in exact agreement with the value reported by Yalcin et al. [11], as discussed above. It is noted that Yalcin et al. used a similar laser energy and optical set-up, and reported a similar coupling of  $\sim 2/3$  of the incident laser energy

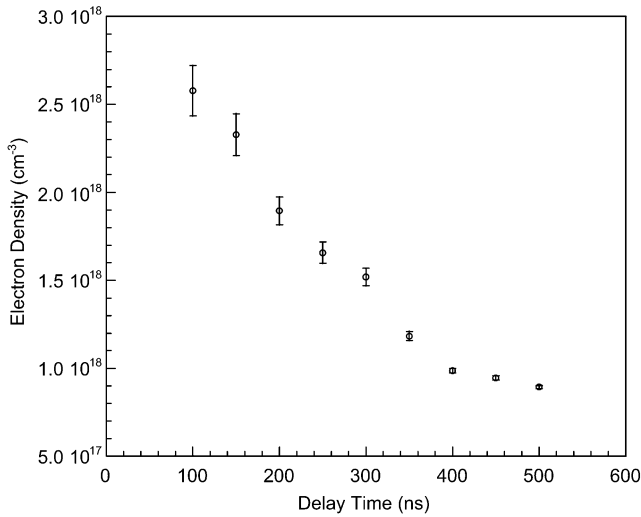


Fig. 3. Free electron number density as a function of time following plasma initiation, as measured using the Stark broadened  $H_{\alpha}$  line width.

into the plasma, which also agrees well with the value measured with the current LIBS setup [15]. Overall, the electron density profile reveals a near linear decay in electron number density between 100 and 400 ns, following by a more gradual decay over the last three data points. This is somewhat in contrast to the non-linear changes in plasma transmission and plasma continuum emission during a similar temporal region, namely between 100 and 400 ns. However, it is noted that the continuum emission is a highly non-linear process (i.e. Planck distribution), while the transmission data must be further reduced to make quantitative comparisons.

The plasma transmission  $\tau$  may be modeled using the Beer–Lambert relationship, namely

$$\tau = \exp\{(\sigma NL)_1 + (\sigma NL)_2 + \dots + (\sigma NL)_n\}, \quad (2)$$

where  $(\sigma NL)_i$  represents the optical depth or turbidity of the  $i$ th species, with  $\sigma$  the absorption cross-section,  $N$  the absorbing species number density, and  $L$  the absorption path length. For the present analysis, it is assumed that free electrons are solely responsible for attenuation of the probe laser beam, which results in the following relation between the measured plasma transmission and the absorption coefficient (defined as  $K_{\text{abs}} = \sigma n_e$ ), namely

$$K_{\text{abs}}L = \ln(\tau). \quad (3)$$

While the absorption cross-section is correctly the sum of the absorption and scattering cross-sections, scattering of the probe laser beam by plasma free electrons, Thomson scattering, is neglected due to the

state of the plasma frequency in relation to the incident frequencies of the probe laser [16]. Specifically, for the first few hundred nanoseconds, the measured electron density is nominally  $2 \times 10^{18} \text{ cm}^{-3}$ , which yields a plasma frequency of  $\sim 10^{13} \text{ Hz}$  using the relation  $\nu_p = 9 \times 10^3 n_e^{1/2}$  [17]. The plasma frequency is the reciprocal of the Debye length and represents the resonance frequency of the free electron oscillations about their equilibrium positions. For the 532 and 1064 nm probe lasers, the corresponding frequencies of  $5 \times 10^{14} \text{ Hz}$  and  $2 \times 10^{14} \text{ Hz}$ , respectively, are sufficiently close to the plasma frequency such that significant absorption is expected, thereby dominating any scattering effects. Eq. (3) enables conversion of the Fig. 1 transmission data to a more quantitative measure of the plasma properties, namely the plasma optical depth or turbidity. The reduced plasma turbidity data and the measured electron density data both represent the temporal evolution of the plasma, hence it is interesting to examine the correlation between these two parameters. To this end, the measured plasma turbidity and electron density data were paired at each similar temporal delay over the range from 100 to 300 ns following plasma initiation. The result is presented in Fig. 4, which reveals a linear relationship between the 532-nm probe laser turbidity and the free electron density ( $R=0.998$ ).

An interesting result of the Fig. 4 data is that based on the assumption of free electron absorption and the additional approximation of constant optical path over this 200 ns time period, the slope of linear fit yields the

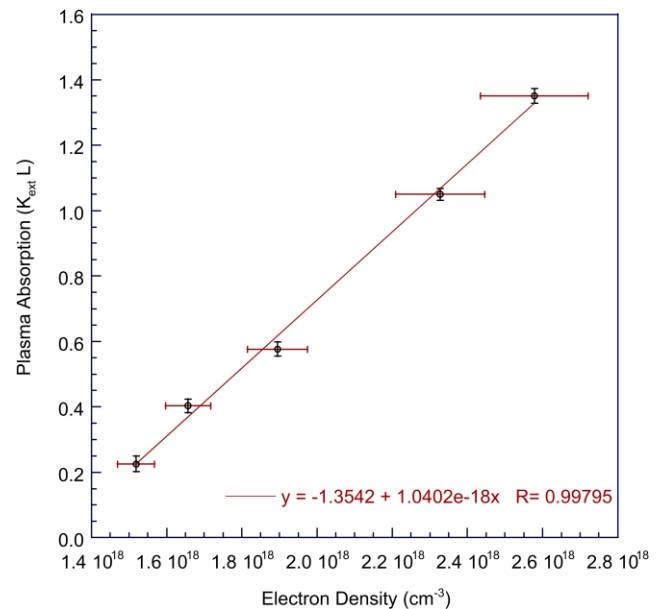


Fig. 4. Measured absorption coefficient for the 532 nm probe laser beam as a function of the corresponding measured free electron density. Each data point corresponds to a specific delay time between 100 and 300 ns following plasma initiation.

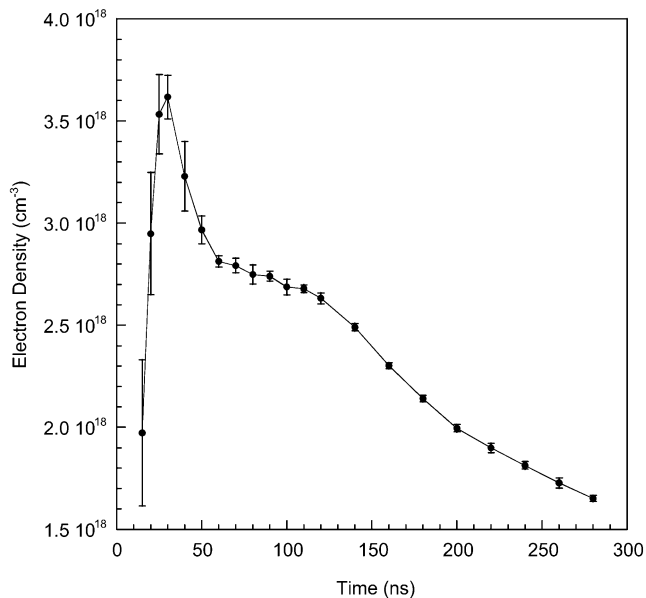


Fig. 5. Predicted electron density values as a function of time following plasma initiation. The data are based on the calculated free-free absorption cross-section of  $9.5 \times 10^{-18} \text{ cm}^2$  and the measured 532-nm transmission data.

free-free (inverse Bremsstrahlung) absorption cross-section. In a complementary recent study, the two-laser approach was used to profile the overall plasma shape under similar experimental conditions [13]. It was reported that by approximately 20 ns following plasma initiation, the plasma had expanded to its characteristic size, with a linear dimension of 1.1 mm along the path of the orthogonal probe laser beam. Using this path length, the calculated free-free absorption cross-section is  $9.5 \times 10^{-18} \text{ cm}^2$  for 532 nm radiation. This value compares very well with a calculated effective absorption cross section of approximately  $3 \times 10^{-17} \text{ cm}^2$  at 500 nm based on the sum of free-bound and free-free cross sections per  $\text{H}^-$  ion [7]. The absorption coefficients  $K_{\text{abs}}$  corresponding to the Fig. 4 data range from 2 to  $12 \text{ cm}^{-1}$ . These values agree very well with theoretical calculations reported for 532 nm radiation in a fully ionized hydrogen plasma [18].

Another interesting result of the measured absorption cross-section is that it enables calculation of electron densities from transmission data at time scales below 100 ns, the lower limit realized in the present study for direct Stark broadening measurements. The extrapolated electron density measurements are presented in Fig. 5 down to 15 ns following plasma initiation. The free electron density profile peaks at 30 ns (corresponding to the minimum in 532-nm transmission) at a value of  $3.6 \times 10^{18} \text{ cm}^{-3}$  and reveals a value of approximately  $2 \times 10^{18} \text{ cm}^{-3}$  at 15 ns delay. It is noted that the delay of 30 ns corresponds to the 99% decay point of the incident laser pulse, hence essentially the full-width.

Accordingly, based on the extrapolation of the measured transmission, the electron density profile peaks at the tail end of the incident laser pulse. Overall, the change in electron number density during the first few hundred nanoseconds of plasma evolution is not that great, hence an aerosol particle engulfed by the plasma is subjected to a relatively consistent frequency of electron-particle collisions. This suggests that the plasma temperature (i.e. electron energy  $\sim$  temperature) could be more important than absolute free electron density for plasma-particle interactions, namely particle dissociation and vaporization.

While temporal regions limited to the first few hundred nanoseconds of plasma evolution are characterized by significant electron densities, plasma frequencies, and plasma absorptivity, as described above, the longer delay times (500 to 1000 ns) reveal a plasma frequency  $\nu_p \sim 10^{12} \text{ Hz}$ . Such a relatively low plasma frequency is consistent with the corresponding near transparency of the plasma to the probe laser wavelengths (i.e.  $\nu_{\text{incident}}$ ), as expected for the condition of  $\nu_p \ll \nu_{\text{incident}}$ .

In summary, the laser-induced plasma investigated in the current study (typical of conditions used for LIBS-based gas and aerosol analysis) is characterized by significant transient changes in electron density and plasma absorptivity during the first few hundred nanoseconds. The fundamental change from an absorbing (i.e. optically thick) plasma to a non-absorbing plasma during this period is important with respect to the radiative transfer within and from the plasma, and is, therefore expected to play a role in the interactions between the laser-induced plasma and incorporated particles. Hence a better understanding of such processes provides a starting point for the more complex plasma-particle interactions, as well as furthering the development of plasma modeling capabilities, and advancing LIBS as an analytical technique.

## Acknowledgments

This work was supported in part by the US Navy Office of Naval Research through contract N00014-0210838, and in part by the National Science Foundation through grant CTS-0317410.

## References

- [1] D.W. Hahn, M.M. Lunden, Detection and analysis of aerosol particles by laser-induced breakdown spectroscopy, *Aerosol Sci. Technol.* 33 (2000) 30–48.
- [2] R.E. Neuhauser, U. Panne, R. Niessner, G.A. Petrucci, P. Cavalli, N. Omenetto, On-line and in-situ detection of lead aerosols by plasma-spectroscopy and laser-excited atomic fluorescence spectroscopy, *Anal. Chim. Acta* 346 (1997) 37–48.
- [3] J.E. Carranza, D.W. Hahn, Assessment of the upper particle size limit for quantitative analysis of aerosols using laser induced breakdown spectroscopy, *Anal. Chem.* 74 (2002) 5450–5454.

- [4] C. Parigger, J.W.L. Lewis, D. Plemmons, Electron number density and temperature measurement in a laser-induced hydrogen plasma, *J. Quantum Spectrosc. Radiat. Transfer* 53 (1995) 249–255.
- [5] C.G. Parigger, D.H. Plemmons, E. Oks, Balmer series  $H_{\beta}$  measurements in a laser-induced hydrogen plasma, *Appl. Opt.* 42 (2003) 5992–6000.
- [6] E. Oks, A new spectroscopic effect resulting in a narrowing of hydrogen lines in dense plasmas, *J. Quantum Spectrosc. Radiat. Transfer* 65 (2000) 405–414.
- [7] H.R. Griem, *Principles of Plasma Spectroscopy*, Cambridge University Press, Cambridge, United Kingdom, 1997.
- [8] H.R. Griem, *Spectral Line Broadening by Plasmas*, Academic Press, New York, 1974.
- [9] A. Borghese, S.S. Merola, Time-resolved spectral and spatial description of laser-induced breakdown in air as a pulsed, bright, and broadband ultraviolet-visible light source, *Appl. Opt.* 37 (1998) 3977–3983.
- [10] M. Villagran-Muniz, H. Sobral, E. Camps, Shadowgraphy and interferometry using a CW laser and a CCD of a laser-induced plasma in atmospheric air, *IEEE Trans. Plasma Sci.* 29 (2001) 613–616.
- [11] S. Yalcin, D.R. Crosley, G.P. Smith, G.W. Faris, Influence of ambient conditions on the laser air spark, *Appl. Phys. B* 68 (1999) 121–130.
- [12] D.W. Hahn, J.E. Carranza, G.R. Arsenault, H.A. Johnsen, K.R. Hencken, Aerosol generation system for development and calibration of laser-induced breakdown spectroscopy instrumentation, *Rev. Sci. Instrum.* 72 (2001) 3706–3713.
- [13] J.E. Carranza, D.W. Hahn, Plasma volume considerations for analysis of gaseous and aerosol samples using laser-induced breakdown spectroscopy, *J. Anal. At. Spectrosc.* 17 (2002) 1534–1539.
- [14] M.A. Gigosos, V. Cardenoso, New plasma diagnosis tables of hydrogen Stark broadening including ion dynamics, *J. Phys. B: At. Mol. Opt. Phys.* 29 (1996) 4795–4828.
- [15] J.E. Carranza, D.W. Hahn, Sampling statistics and considerations for single-shot analysis using laser induced breakdown spectroscopy, *Spectrochim. Acta Part B* 57 (2002) 779–790.
- [16] K. Warner, G.M. Hieftje, Thomson scattering from analytical plasmas, *Spectrochim. Acta Part B* 57 (2002) 201–241.
- [17] A. Thorne, U. Litzen, S. Johansson, *Spectrophysics Principles and Applications*, Springer-Verlag, Berlin, 1999.
- [18] H. Hora, H. Wilhelm, Optical constants of fully ionized hydrogen plasma for laser radiation, *Nucl. Fusion* 10 (1970) 111–116.